A Reflection Grating Spectrometer for the X-Ray Multi-Mirror (XMM) Space Observatory: Design and Calculated Performance

Michael C. Hettrick and Steven M. Kahn

Proc. Soc. Photo-Opt. Instr. Eng. vol. 597, pp. 291-300 (1986)

http://dx.doi.org/10.1117/12.966594

A Reflection Grating Spectrometer for the X-Ray Multi-Mirror (XMM) Space Observatory: Design and Calculated Performance

Michael C. Hettrick* and Steven M. Kahn**

*Lawrence Berkeley Laboratory, Center for X-Ray Optics B80-101, Berkeley CA 94720 USA

**University of California, Department of Physics, Berkeley CA 94720 USA

Abstract

We present a spectrometer design candidate for the X-ray Multi-Mirror (XMM) observatory, being planned by the European Space Agency (ESA) as a long-lived large-area array of telescopes. The science requirement of moderate resolution ($E/\Delta E \sim 100$) spectroscopy in a two octave region (0.5-2 KeV) with extremely high throughput (effective area > 500 cm^2) results in the use of grazing incidence reflection gratings. Due to the low image quality of the telescopes ($\sim$ 1 minute of arc), the grating dispersion must be maximized by use of the classical grating mount in which the spectrum is dispersed within the plane of incident radiation. Due to the small field of view afforded by the x-ray telescopes, the gratings must be situated in the converging beam at the exit of the telescope. A spectrometer module consists of a thin-foil conical mirror telescope, a stack of plane varied-space reflection gratings and an imaging proportional counter. This system is analyzed on the basis of dispersion, geometric aberrations and efficiency. At a spectral resolution of 0.15 Å, a twenty module XMM would attain an average effective area of $\sim$ 900 cm^2, reaching twice this value at the peak wavelength (15 Å). Similar throughput is obtained in second order centered at 7.5 Å, the two spectral orders separated by the non-dispersive energy resolution of the proportional counter. Continuous spectra are obtained in the 6-25 Å band (0.5-2 KeV), and can be extended to 45 Å if desired by tuning of the grating. The instrument sensitivity is sufficient to allow the first spectral detection of soft x-ray features in external galaxies, with access to an estimated population of several hundred active galactic nuclei. Such observations will expand vastly the roles feasible for spectroscopy in x-ray astrophysics, marking the beginning of a new era in space astronomy.

Introduction

Spectroscopy has had a fundamental impact in a number of scientific disciplines. Some of the most far reaching consequences have been repeatedly obtained in the field of astrophysics. However, to date, spectroscopy of cosmic sources has been practical as a routine method only at visible, infrared and radio wavelengths. Astronomical observations in the ultraviolet and x-ray must be performed above the Earth's absorbing atmosphere, which is both costly and problematic. The instrumentation becomes even more technically challenging at the shortest wavelengths, and is further complicated in the case of spectroscopy. Only two grating spectrometers have flown aboard x-ray observatories: the objective grating spectrometers (OGS) on Einstein[1] and EXOSAT[2]. Apart from solar research, these two missions plus a handful of small rocket experiments comprise a total of only a few dozen spectra on cosmic sources at soft x-ray energies ($\sim$ 0.1-2 KeV; 6-124 Å). At present, x-ray astrophysics is truly still in its infancy.

The limited spectroscopic data available is, however, enticing. A particularly inviting spectral band appears to be in a two octave region centered near 1 KeV (12 Å), which includes the K-shell transitions of all ions of C, N, O, Ne and Mg and the L-shell transitions of ions of Ni and Fe. For example, FeXVII lines between 15 and 17 Å have now been detected in four of the five x-ray binary systems observed with the Einstein OGS[3-5]. While this and other data[5-7] have yielded useful results, the small effective collecting area of these instruments (< 1 cm^2) has restricted their use to the brightest sources in the x-ray sky (e.g. Scorpius X-1). If spectroscopy is to have the level of impact on soft x-ray astronomy which it has had at longer wavelengths, vast increases in sensitivity will be required. To sample a typical population of objects - galactic as well as extra-galactic, a gain of four orders of magnitude (10^4) over the Einstein OGS is necessary. This implies not only an enormous increase in collecting area (a factor of $\sim 10^3$ being technically feasible) but also an observatory-class mission dedicating a large fraction of its observing time to spectroscopy.

ESA plans to launch such a large-scale long-lived x-ray satellite, the XMM[8], by the year 2000. To achieve the requirement for large area, XMM will consist of an array of low resolution ($\sim$ 1 minute of arc) telescopes. This resolution severely limits the choice of spectrometer, as the spectral resolution of any dispersing optic degrades linearly with the angular resolution of the object. Proper interpretation of the spectra in the soft x-ray band 6-25 Å is crucial and requires continuous exposure of the entire spectrum with a

spectral resolution of $\lambda/\Delta\lambda \sim 100$ or greater. This resolution requirement is inconsistent with the use of transmission gratings unless the telescope angular resolution is improved by a factor of six, to 10 seconds of arc. The simultaneous requirement of dispersing with high area over a wide bandpass (100 resolution elements) precludes the use of scanning optics such as crystals. Therefore, the types of spectroscopic instruments employed on Einstein or EXOSAT and planned for other high resolution telescopes are not suited to XMM. Even the off-plane (conical) reflection grating mount is incapable of meeting the resolution requirement unless groove densities of order 1.5×10^4 mm^{-1} can be fabricated with near theoretical efficiency over large grating surfaces. This groove density is a factor of 3-5 above the current level of technology. The combined requirements of high efficiency, high dispersion and wide bandpass lead to the choice of grazing incidence reflection gratings which disperse in the high dispersion mode (grooves normal to the plane containing both incident and diffracted light). This classical mounting has been in existence for several hundred years, and because of its unique ability to generate high dispersion, has retained its predominance even at grazing incidence. In a preliminary feasibility study[9] we have discussed in detail the various reflection grating designs available for use on an XMM class observatory. Since that time, significant progress has been made by ESA[10] in identifying the type of telescope design likely to be used. This has made it possible to now specify the optimum spectrometer configuration, the details of which are presented in the following sections of this paper.

Design Choice

As the XMM will be used for observations of both soft ($\sim$0.5-2 KeV) and hard ($\sim$7 KeV) x-rays, the telescopes must accomodate both functions. It is highly desirable to use a single design for each of the 20 modules residing on the observatory (Fig. 1), for reasons ranging from cost to ease of calibration. The thin-foil conical mirror system originally proposed by Serlomitsos[11] has been identified as the prime candidate for the telescope design. Each system consists of a nested set of short cones which approximate the familiar Wolter I telescope. To obtain useable reflectance at 7 KeV, the maximum graze angle must be $< 0.5^o$. Thus a full-scale XMM observatory would consist of twenty telescopes, each of approximately 50 cm diameter and containing 100 foil cones with a focal length of approximately 8 meters[8]. A prototype of such a telescope has in fact been built and tested[12], having a somewhat smaller focal length and correspondingly larger graze angle. Because the individual mirror cones are quite short (10-20 cm), the off-axis resolution is essentially equal to the on-axis value. However, due to the shallow graze angle, vignetting is substantial. The field of view θ_i for the i'th mirror cone is :

$$\theta_i \text{ (full width)} = 2\,\gamma_i \tag{1}$$

where γ_i is the graze angle for the i'th cone. The widest field is thus $\sim 0.9^o$ for the outer cone ($\gamma \sim 0.45^o$), corresponding to a FWHM of only $\sim 0.45^o$. Summing over all cones, the net FWHM is even smaller. Since the telescope resolution is not expected to be better than approximately ε=1 min of arc, the vignetting introduces a fundamental limit to the number of resolution bins within the telescope field:

$$\text{No. Telescope Bins} < 2\gamma_{max}/\varepsilon \equiv N_T \tag{2}$$

or approximately 50; only half this under the FWHM response. This can be increased only by decreasing ε (not technically feasible) or by increasing γ_{max} which would abruptly diminish the throughput at 7 KeV and above. Neither of these two options is appealing. While for spatial imaging the total number of 2-D resolution elements within the field of view is still respectable ($\sim$2000), for dispersive spectroscopy the result would at first appear catastrophic. In the simple objective spectrometer configuration where the gratings are placed at the telescope entrance and disperse various wavelengths into the telescope, the optimum spectral resolution is

$$\begin{aligned} \Delta\lambda &= (\lambda_{max}-\lambda_{min})/N_T \\ &> (\lambda_{max}-\lambda_{min})\varepsilon/2\gamma_{max} \end{aligned} \tag{3}$$

or 0.3-0.6 Å over a first order spectrum from 10-25 Å. This represents a resolving power of only 25-50 at the center of the spectrum. This is insufficient to meet the scientific objective of $\lambda/\Delta\lambda \sim 100$ or larger. The latter requires at least 100 resolution bins within the field of view, preferably within the FWHM of the on-axis response.

However, if the gratings are located in the converging beam at the telescope exit, this constraint disappears, and the telescope is used on-axis at all wavelengths. Grazing incidence plane reflection gratings have been designed and recently used in converging beams of soft x-ray/extreme UV radiation[13-15]. By use of a smooth variation in the groove spacings, these designs correct for the geometric aberrations which would otherwise result from the converging beam configuration. Unlike conventional grazing incidence gratings,

the varied line-space (VLS) grating also images the spectrum on a normal incidence focal plane, which matches the imaging surface available with electronic detectors such as imaging proportional counters. The use of VLS converging beam reflection gratings has been required in other astronomy missions as well (EUVE[15] and LAMAR[9]) due to unacceptable offaxis response of various grazing incidence telescopes.

A grating module would be incorporated on XMM as illustrated in Fig. 2, residing in the cavity between the foil telescope and the detector. As the gratings divert light away from the telescope axis, there would be in addition one detector per telescope dedicated to spectroscopy (see also Fig. 1). In Fig. 3 we show the arrangement of gratings within a module, consisting of a stack of identical replicas from a single grating master. An analogous geometry in the case of normal incidence transmission gratings is the "facet-type" array[16] in which each grating panel or facet is identical but displaced from adjacent panels along a non-closed surface. Each grating module shown in Fig. 3 collects 50% of the incident light, the remaining 50% left untouched for broadband imaging or a complementary focal plane instrument. As illustrated in Fig. 2, each grating module could be mounted on a pivot (e.g. flexure hinge) permitting small ($\pm 3^{o}$) rotations. For non-spectroscopic observations, a rotation of the grating module by $\sim 1.5^{o}$ would bring the grating planes all parallel to the incident converging beam resulting in passage of almost all the telescope light through the grating stack as in a venetian blind. In addition, such grating pivot could be used in the opposite sense to increase the grating graze angles and thereby extend the spectral bandpass to longer wavelengths (e.g. 25-45 Å).

Detailed Design and Performance Characteristics

In table I we list design parameters for an optimized grating array and proceed to calculate the expected instrument performance.

Table I. Critical Design Parameters

Telescope: nested conical thin-foils	Grating Module: planar stack, varied spacings, mechan. ruled, reflection
Diameter ... 500 mm	
Focal length ... 8000 mm	Average groove density ... 500 mm^{-1}
Max. graze Angle ... 0.45^{o}	Ruled width ... 200 mm
Image diameter on-axis ... 1.0 arcmin	Groove length ... 250 mm
Overcoating ... gold	Blaze angle ... 0.6^{o}
	Spectral order ... -1, -2 (inside)
	Plate scale ... 0.14Å/mm, 0.07Å/mm
Detector: Imaging proportional counter	Bandpass ... 10-25 Å, 5-13 Å
	Substrate ... 1 mm beryllium
Aperture ... 120 mm	Surface replica ... gold
Window ... 1 μm polypropylene , 80% mesh	Surface flatness ... 100 fringes at 6328 Å
Spatial resolution ... 0.5 mm	
Energy resolution ... FWHM = $0.4\ E^{-\frac{1}{2}}$(KeV)	
Non x-ray background (using energy res.) ... 0.01 cnts $cm^{-2}sec^{-1}E^{-\frac{1}{2}}$(KeV)	Grating focal distance ... 7500 mm Grating facet graze angle ... 2^{o}

Resolution/Efficiency Trade-Off

Due to the finite size image produced by the telescope (Fig. 4), the spectral resolution of the convergent beam grating will be limited as previously given[9]:

$$\lambda/\Delta\lambda = E/\Delta E = |\eta - 1|\ \sin\gamma\ (L/F)\ [\eta^2\varepsilon^2 + (\Delta x_D/F)^2]^{-\frac{1}{2}} \qquad (4)$$

$$= L\ |\eta - 1|\ \sin\gamma\ [\eta^2\Delta x_T^2 + x_D^2]^{-\frac{1}{2}}$$

where γ is the graze angle relative to a groove facet, F is the focal length of the telescope, ε its image quality (diam in radians), Δx_T the corresponding image FWHM at the detector, L the grating focal length, η its blaze efficiency and Δx_D the detector resolution. Due to groove shadowing, $\eta < 1$, but is typically greater than 0.5 if care is taken to use a blaze angle optimized for this in-plane geometry. In the present case, using the parameters from table I result in a blaze efficiency $\eta \sim 0.53$ for a resolving power of 100 at a wavelength of 15 Å. Such high groove efficiencies have been experimentally verified for a grazing incidence VLS grating in the extreme UV[15]. At our groove density of only 500 g/mm, the required shallow blaze angle of 0.6^{o} corresponds to a groove depth of approximately 200 Å. This is comparable in its requirements on ruling accuracy as a 2400 g/mm grating with 3^{o} blaze angle - a popular grating commonly ruled on existing engines. Ruled gratings with 1^{o} blaze angles are in fact available as stock items.

In Fig. 5 we plot the spectral resolution and groove efficiency (neglecting reflectance) as functions of the wavelength for both the first and second spectral orders. The resolution is derived from equation 4, and the groove efficiency was calculated using a phenomenological formula which has been previously shown to agree with experimental data to within ∿ 5%.[15] Despite the effect of groove shadowing on the peak efficiency, the groove efficiency is in the range 35-53% over the desired band 6-25 Å. The decline is gradual longward of the first order peak at the blaze wavelength of 15 Å, which is due to the groove shadowing: an effect which partially offsets the decrease in peak intensity. The spectral resolution in first order is 0.15 Å, which is a resolving power of 100 at 15 Å, or 115 near the band center. In second order, the resolution is 0.075 Å which also meets the resolution requirement over the 6-13 Å band. The two orders are separated non-dispersively by the energy resolution of the proportional counter detector[17] (see table I). At 15 Å this resolution is approximately 50% and at 7.5 Å is approximately 35%. This is sufficient to separate orders 1 and 2, but cannot be extended to spectral order 3 or higher without ambiguity.

As the gratings are situated downstream of the telescope and its dominant aberration, the use of an inside spectral order is crucial[14], resulting in a de-amplification of the telescope image size by a factor η^{-1}. As shown in Fig. 4, this effect produces a spectral image width of only 1.2 mm while that of the direct telescope image is 2.4 mm. This makes it possible not only to meet the requirement of spectral resolution, but also to fit the entire spectral band (∿ 100 wavelength bins) within the same detector aperture (120 mm) as used by the telescope for non-spectroscopic imaging.

Geometric Aberrations

A major design consideration is the wavefront distortion caused by the convergent beam geometry, i.e. the grating aberrations. In generating Fig. 4, these were assumed to be small. These aberrations can arise in two ways: 1) the aberrations of an individual grating in the stack, and 2) the aberrations produced by inequality of dispersion between different gratings.

The first term, inherent aberration of a single grating, is made to vanish for the central grating in a stack by appropriate choice of groove space variation[13,14], approximately 11% across the 200 mm ruled width. Because this functional variation is determined predominantly by the angle of incidence and the grating width, all gratings require approximately the same variation if they are each placed at the same angle relative to the incident light. Thus, as shown in Fig. 3, each grating is tilted slightly relative to adjacent ones, but only half as much as required in a mirror telescope (e.g. Kirkpatrick-Baez system). The grating module is thus greatly simplified by use of identical replicas which for the purposes of alignment can be treated as mirrors. As each grating is a slightly different distance from both the telescope focus and the spectrum, there will be some residual aberrations due to the asymmetry. After writing the light-path function and employing Fermat's principle, the dominant aberrations are determined:

$$\Delta x/w = \left|\sin^2\beta\ [\cos(2\gamma)-\cos(2\gamma+\phi)] - \tfrac{1}{2}\phi^2\sin^2\alpha\right|/\sin\beta \qquad (5)$$

$$\Delta y/\ell = 2\left|1 - \cos(2\gamma)/\cos(2\gamma-\phi)/\cos\phi\right| \qquad (6)$$

where Δx is the aberrant image width, Δy the aberrant image height (astigmatism), α the angle of glancing incidence (∿ 1.5°), β the glancing angle of diffraction (∿ 3°), ϕ the half-cone angle of the converging telescope beam (∿ 1.8°), w the grating ruled width (200 mm) and ℓ the groove lengths (∿ 250 mm). Thus we determine $\Delta x \cong 0.05$ mm, which is negligible in comparison to the detector pixel of 0.5 mm or the dispersive width of 1.2 mm shown in Fig. 4. Equation 6 requires the spectroscopy detector to lie approximately 23 mm above the image plane of the telescope (see Fig. 2), and includes the combined groove length 2ℓ for grating pairs near the center of the telescope (diam 500 mm). The astigmatism is only $\Delta y \cong 0.75$ mm which is small compared to the telescope contribution of 2.4 mm to the image height. If the spectroscopy detectors were placed on the same plane as the telescope detectors, the astigmatism aberration is calculated to be:

$$\Delta y/\ell = 2\left|1 - \cos\phi/\cos(2\gamma+\phi)\right| \qquad (7)$$

or $\Delta y \cong 2.8$ mm. Approximating the telescope image profile as a normal distribution function with FWHM of 2.4 mm, the convolution of 2.8 mm astigmatic aberration with the telescope resolution of 1 minute of arc is an error function with FWHM of still only 3 mm, as plotted in Fig. 4.

The second aberration term, that due to differences in dispersion between gratings in the stack, will displace the centers of the images by an amount which we calculate to be:

$$\Delta x = 8\ \phi\ \gamma^2\ L \qquad (8)$$

where L is the grating-detector average separation, and where it is assumed that the graze angle at the grating center γ is exactly equal for all gratings in the stack. This leads to an aberration of approximately 2 mm in spectral width, which is unacceptably large compared to the 1.2 mm width corresponding to the desired spectral resolution. To remove this dominant term in the dispersion aberration requires that the graze angles γ vary slightly from grating center to grating center across the stack. The fractional change is

$$\Delta\gamma/\gamma \cong 4\ \gamma\ \phi \tag{9}$$

across the entire module, or approximately 0.5 arcminutes. Thus, although formally inconsistent with the assumption used to compute the individual grating aberrations, the quantitative change in those previous results is found to be negligible. Dispersively, the advantage of this slight deviation in the grating orientations is that it would force all gratings to have the same image centroids at the center of the detector, changing eq'n 8 to:

$$\Delta x = 8\ \phi\ \gamma\ |x| \tag{10}$$

where x is the image distance from the detector center. At the edges of the spectrum, $x = \pm 60$ mm and we find $\Delta x \cong 0.5$ mm. This can be reduced a factor of two further by tilting the spectroscopy detector so as to bring its imaging surface perpendicular to the ray dispersed from the center of the grating module, rather than being perpendicular to the telescope axis (approximately a 4^{o} tilt would be required). The resulting aberration due to dispersion inequality between gratings at opposite edges of the module would in that case be only approximately 0.25 mm, which is negligible in comparison to the contribution from the telescope.

As a practical matter, we note that the grating planes are assumed for the purpose of this analysis to be co-aligned to within a small fraction of the telescope angular resolution. Due to the image quality of the telescope ($\sim$ 1 minute of arc), this should not represent a serious challenge. In fact, alignment techniques have been developed for mirror stacks[17] at this resolution, but are significantly more complex in that the mirrors are also bent into optimum shapes. With our use of plane (grating) surfaces, the mounting structure within the grating module should be straightforward.

Effective Area

In Fig. 6 we plot the net effective area of a spectrometer (consisting of a telescope, grating module and detector) as well as that for a full-up 20 module XMM spectrometer array. In calculating the spectrometer efficiency, we have included the groove efficiency plotted in Fig. 5, the reflectance of a gold overcoating at 2^{o} graze angle as given by Henke[18] and the quantum efficiency of a proportional counter with 1μm polypropylene window[17] ($\sim$ 10% at 30 Å, $\sim$ 30% at 20 Å and $\sim$ 65% at 10 Å). The effective area of the assumed thin-foil telescope is given by Bleeker et al[8] as 1100 cm^2 for wavelengths greater than 6 Å; since only half of each telescope is used for spectroscopy, we have assumed only 550 cm^2 per module to obtain the curves in Fig. 6. We have also assumed a small obscuration (20%) due to grating substrates of finite thickness (1 mm). As the total grating surface per module is approximately 4×10^4 cm^2 (50 gratings), weight considerations have also encouraged us to minimize the grating thickness as well as the density of material. We have considered various methods of fabricating thin, lightweight relatively flat ($\sim$ 0.5 minutes of arc or better) grating replicas. Our current plan is to use 1 mm thick sheets of beryllium which would obscure only 20% of the incoming beam and weigh only 7 kg per grating module plus the weight of the mounting structure. However, we are also currently investigating new grating replication techniques to meet the general need for large numbers of gratings.

In Fig. 6 we have shown the results for both the first and second spectral orders. A single XMM module is seen to deliver an average effective area of $\sim$ 50 cm^2 over the 6-25 Å region, peaking at 65-75 cm^2 at the blaze wavelengths of 7.5 Å and 15 Å. A full twenty modules would deliver 900 cm^2 on average. The rapid fall in effective area at the shortest wavelengths (< 7 Å) is the result of dying reflectance off the grating, while the decline at the longest wavelengths in first order is due largely to the thick window assumed for the proportional counter. The effective area for wavelengths longward of 25 Å (e.g. 25-40 Å) can be made appreciable by use of a thinner (0.5μm) detector window. It is sobering to note that the effective area in the 15-17 Å region, one of high scientific return on Einstein, is approximately 1400 cm^2: approximately 2000 times larger than available with the Einstein OGS, whose effective area[1] is also plotted in Fig. 6 for comparison (an average of the 500 ℓ/mm and 1000 ℓ/mm gratings has been taken). Even if only ten of the anticipated twenty XMM telescopes were to be outfitted for spectroscopy, the gain compared to Einstein would be the desired factor of 1000. Furthermore, XMM is expected to spend a large fraction of its observing time on spectroscopic targets, with a typical long observing time of 10^5 seconds ($\sim$ 1 day) not being unreasonable.

Potential Observations

Given an effective area curve $A_e(\lambda)$ it is easy to determine the sensitivity of this instrument to spectral lines, assuming we are not limited by any source of background:

$$I_\lambda(\text{photons cm}^{-2}\text{s}^{-1}) = 10^{-4}S^2/A_e(\lambda)/T_4 \qquad (11)$$

where S is the sigma-level of the detection (e.g. S=5 is a 5σ detection) and T_4 is the observing time in units of 10^4 seconds (∿ 3 hours). For example, even an extremely short observation (T_4 = 0.1) would allow the 5σ detection of spectral lines at a threshold of only ∿ 3×10^{-5} ph/cm²/sec. With such an instrument, high statistical quality spectra can be obtained on thousands of stellar coronae in a matter of weeks. Due to the short observing time required, the detector background can be ignored. For example, multiplying the value given in table I by 20 (the number of proportional counters recording a spectrum) and by the area enclosed by an image (∿ 0.03 cm²) one expects a non x-ray background of only ∿ 6 counts in each resolution bin near 15 Å for one thousand seconds of observing time. However, it is crucial to understand that this low background is the result of using the energy resolution of a proportional counter detector to accept only those events which fall within its discrimination level in pulse height. A detector with little or no energy resolution would exhibit a background approximately 10 times more intense, giving rise to background-limited sensitivity after only a few hundred seconds of observing. With the proportional counter, the observation of stars is a comparatively simple task for an XMM spectrometer.

The most challenging, and perhaps most interesting, astrophysical observation which XMM can make at soft x-ray wavelengths is the spectral detection of features in the continua of active galactic nuclei (AGNs). These are believed to be accretion-powered sources similar to the intense x-ray binaries (galactic objects) whose spectra were detected with the Einstein OGS[3-7]. For such sources, there is a pervasive continuum consisting of many features whose positions and profiles cannot be easily predicted. The complex physics of these sources prevents a simple deconvolution of the spectrum as the sum of a featureless continuum and a series of discrete lines at known wavelengths. Rather, meaningful interpretation of spectra from AGNs will almost certainly require the fitting of a model to a large spectral region (e.g. one octave in wavelength). As the continuum will dominate the statistical quality of the data, the detection threshold for a spectral line can be written in terms of its equivalent width in Ångstrom units W_λ:

$$W_\lambda(\text{Å}) = S\,[A_e(\lambda)]^{-\frac{1}{2}}\,T^{-\frac{1}{2}}\,(12.4)^{\frac{1}{2}(\Gamma-1)}\,\Delta\lambda^{\frac{1}{2}}C^{-\frac{1}{2}}\,\lambda^{1-\frac{1}{2}\Gamma}\,e^{\frac{1}{2}N_H\sigma(\lambda)} \qquad (12)$$

where S is the sigma-level of detection, $A_e(\lambda)$ is the curve of effective area, Δλ and λ are the bin size and wavelength in units of Å. The astronomical quantities are the spectral index of the continuum Γ, its intensity C at 1 KeV in units of photons/cm²/sec/KeV, the intervening column density of neutral hydrogen N_H in units of atoms/cm², and the photon cross-section per atom of intervening material σ(λ) as a function of wavelength in units of cm². The spectral bin size of the spectrometer is Δλ=0.15 Å in first order and 0.075 Å in second order. In addition, the spectral index is known to be approximately Γ = 1.7 for these sources[19]. We demand a five sigma detection for any one bin so as to ensure the probablity of a spurious detection anywhere among the 200 spectral bins is less than 0.01%. From broadband x-ray measurements we know C = 0.02 for one of the ten brightest AGN (3C 273)[19], and the column density is estimated to be $N_H \sim 2\times10^{20}$ cm⁻². Thus we can rewrite equation 12 as:

$$W_\lambda(\text{Å}) = b\,[A_e(\lambda)]^{-\frac{1}{2}}\,T_4^{-\frac{1}{2}}\,\lambda^{0.15}\,e^{10^{20}\sigma(\lambda)} \qquad (13)$$

where T_4 is in units of 10^4 seconds observing time; b ≅ 0.332 for first order spectra and b≅0.236 for second order spectra. Assuming values of σ appropriate to a neutral interstellar medium, and using the effective area for a 20 module spectroscopic observation, we show as Fig. 7 the detectable equivalent widths for spectral lines after a 1 day period of observation T_4 = 10. Over the targeted band of 6-25 Å, the sensitivity is at the 5 mÅ level. Since a number of features at the level of 200 mÅ could be seen in spectra of similar sources (x-ray binaries)[5], an XMM spectrometer array of the type proposed here could detect soft x-ray spectral features at a scientifically meaningful level for AGNs a factor of approximately 6 = (200mÅ/5mÅ)² weaker than 3C 273. As the population of these sources scales as $C^{-3/2}$, and there are approximately 10 AGNs at the strength of 3C 273, the estimated number of AGNs among which XMM could choose as soft xray spectroscopy targets exceeds 100. It is clear that such observations would be unfeasible with a spectrometer of less than approximately 1000 cm², due to the long observing times required and the background-limited nature of the observations.

For comparison we have also carried out similar calculations on the minimum detectable equivalent widths for the AGN 3C120. As shown in Fig. 7, the larger column (10^{21} cm⁻²) to this source results in an interstellar absorption edge from oxygen at 23.3 Å, and a large

decrease in sensitivity longward of the edge due to absorption by interstellar nitrogen ($\sim$ 30 Å) and carbon ($\sim$ 45 Å). While having the potential to yield some measure of the relative abundance and ionization state of these elements in the interstellar (and perhaps circumsource) medium, the basic effect of such absorption is to lower the sensitivity of spectra by large amounts longward of approximately 25-30 Å. This has been observed in the Einstein OGS data on x-ray binaries[3-5], and results in an effective long wavelength cutoff in the detection of soft x-ray spectra from any but the most nearby objects.

Acknowledgements

This work was supported in part by a NASA Innovative Research Grant to UCB. MCH also acknowledges support from the U.S. Department of Energy, Office of Basic Energy Sciences Contract No. DE-AC03-76SF00098. The authors wish to thank Dr. James Underwood for helpful discussions.

References

1. F.D. Seward et al, "Calibration and efficiency of the Einstein objective grating spectrometer," Appl.Opt., Vol. 21, p. 2012. 1982.
2. A.C. Brinkman et al, "Efficiency and resolution measurements of x-ray transmission gratings between 7.1 and 304 Å," Appl.Opt., Vol. 19, p. 1601. 1980.
3. S.M. Kahn, F.D. Seward and T.Chlebowski,"High Resolution Soft X-Ray Spectra of Scorpius X-1: The Structure of Circumsource Accreting Material," Ap.J.,Vol 283,p 286. 1984.
4. S.D. Vrtilek, S.M. Kahn, F.D. Seward, J.E. Grindlay and D.J. Helfand, " X-Ray Spectral Variations in Cygnus X-2: Structure in the Circumsource Medium," Ap.J. (in press).
5. S.D. Vrtilek, S.M. Kahn and D.J. Helfand, "X-Ray Spectroscopy of galactic Bulge Sources," in preparation.

6. C.R. Canizares, "X-Ray Plasma Astrophysics," in Proc. Course and Workshop on Plasma Astrophysics, Vienna Italy, August 1984.
7. R.Mewe, "Soft X-Ray Spectroscopy with EXOSAT," in Proc. 8th Int. Coll. on UV and X-Ray Spectroscopy of Astrophysical and Laboratory Plasmas ed. G. Doschek, Washington DC, 27-29 August 1984, pp. 59-66.
8. J. Bleeker et al, "The XMM Observatory," Physica Scripta, Vol. T7, p. 224. 1984.

9. S.M. Kahn and M.C. Hettrick, "The Application of Reflection Gratings to a Large Area X-Ray Spectroscopy Mission: A Discussion of Scientific Requirements and Various Design Options," Proc. ESA Workshop on a Cosmic X-Ray Spectroscopy Mission, Lyngby. 1985.
10. J. Bleeker, ed. Proc. ESA Workshop on a Cosmic X-Ray Spectroscopy Mission, Lyngby. 1985.
11. P. Serlemitsos, NASA Technical Memorandum 83848, p. 411. 1981.
12. R. Petre and P.J. Serlemitsos, "Conical imaging mirrors for high-speed x-ray telescopes," Appl.Opt., Vol. 24, p. 1833. 1985.
13. M.C. Hettrick and S. Bowyer, "Variable Line-Space Gratings: New Designs for Use in Grazing INcidence Spectrometers," Appl.Opt., Vol. 22, p. 3291. 1983.
14. M.C. Hettrick, "Aberrations of Varied Line-Space Gratings in Converging Light Beams," Appl.Opt., Vol. 23, p. 3221. 1984.
15. M.C. Hettrick et al, "Extreme ultraviolet explorer spectrometer," Appl.Opt., Vol. 24, p. 1737. 1985.
16. K.P. Beuermann, H. Braeuninger and J. Truemper, "Aberrations of a facet-type transmission grating for cosmic x-ray and XUV spectroscopy," Appl.Opt., Vol. 17, p. 2304. 1978.
17. P. Gorenstein, D. Fabricant and L. Cohen, "The LAMAR Telescope Module for High-Throughput Imaging and Spectroscopy," Proc.ESA Work.Cos.X-Ray Spec.Mission. 1985; priv.comm.
18. B.L. Henke et al, "Low-energy x-ray interaction coefficients: Photoabsorption, scattering and reflection," Atom. Data Nucl. Data Tables, Vol. 27, p. 1. 1982.
19. J.P. Halpern, "X-Ray Spectra of AGN," dissertation Harvard University. 1982.

X-RAY MULTI-MIRROR ARRAY

CONCEPTUAL REPRESENTATION

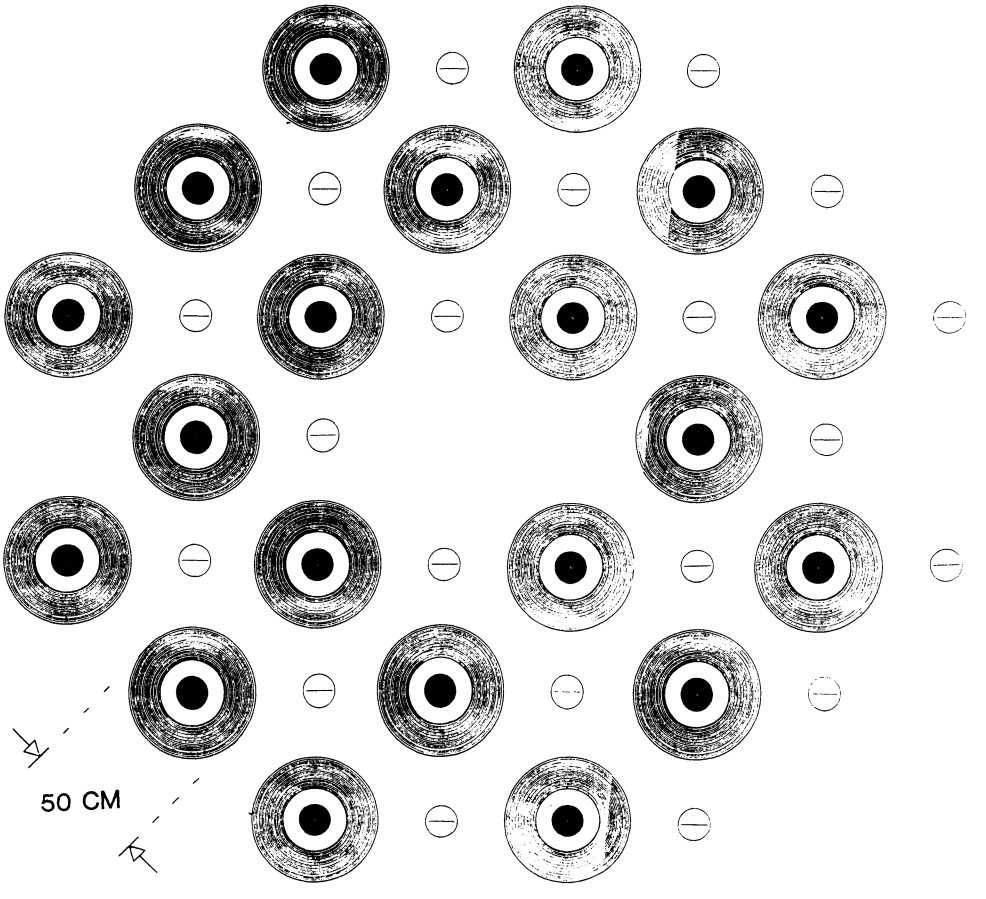

Fig. 1. Array of twenty telescopes comprising the XMM observatory, as viewed along the optical axis. In this conceptual representation, each telescope is assumed to consist of a large number (∿ 100) thin foil cones filling an aperture diameter from 25 cm to 50 cm. Each telescope provides spatial imaging on its own on-axis detector, drawn to scale here as a filled circle. In addition, soft x-ray spectra would be imaged on dedicated detectors, illustrated here as open circles divided by linear spectra. An actual XMM observatory would be more closely packed than the exploded view shown here for clarity.

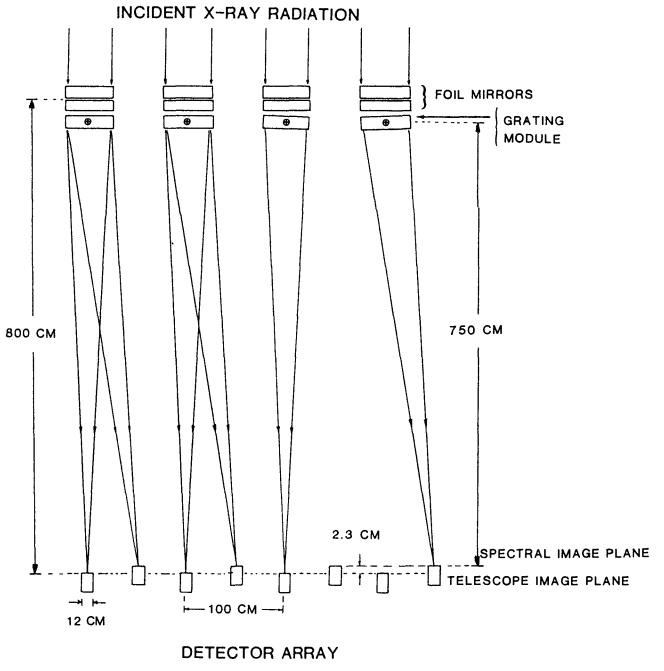

Fig. 2. Cross-sectional view of four telescope-spectrometer modules. A grating module is placed in the convergent light from each telescope, dispersing a soft x-ray spectrum to detectors placed near the focal plane of the telescope. A small (1-2°) pivot of a grating module can act as a venetian blind, either to allow direct passage of the telescope beam or to tune the spectral bandpass falling on the detector. Not to scale.

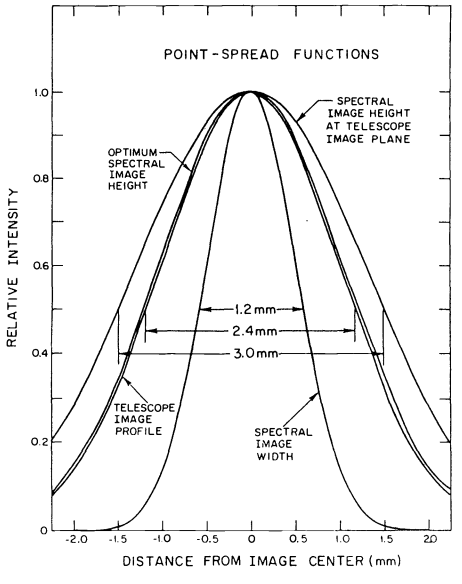

Fig. 4. Images profiles calculated at the detector in two directions. The tele scope on-axis response is assumed Gaussian. The gratings de-magnify to 1.2 mm the 2.4 mm telescope FWHM arising from a mirror figure of 1 arcminute.

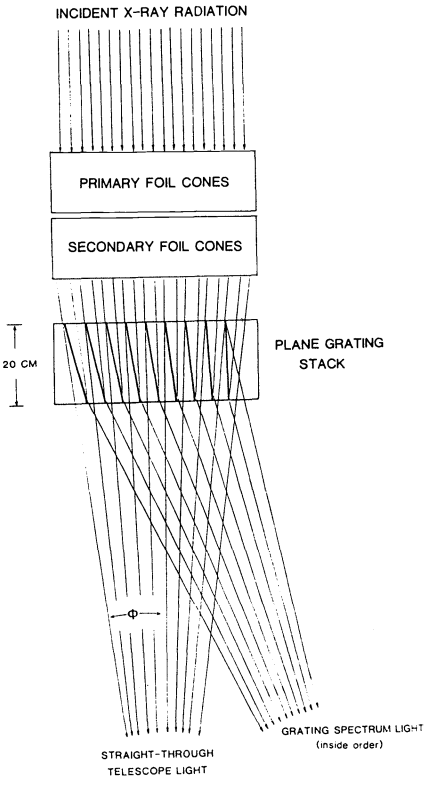

Fig. 3. Detail of grating module, which picks off 50% of the incident beam. Only a small number of gratings are shown at exaggerated graze angles.

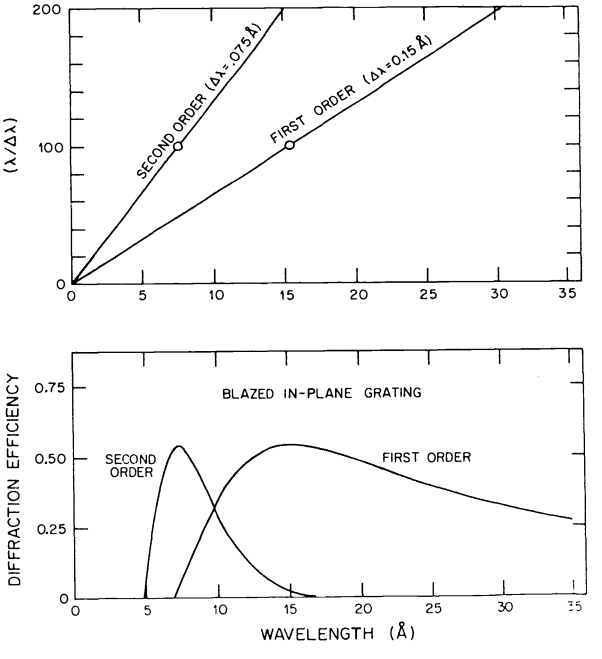

Fig. 5. Calculated resolving power (top panel) assuming a telescope resolution of 1 arcminute. The resolution is 100 at the blazed wavelengths (circles). Calculated grating efficiency (bottom panel) does not include reflectance of the gold coating.

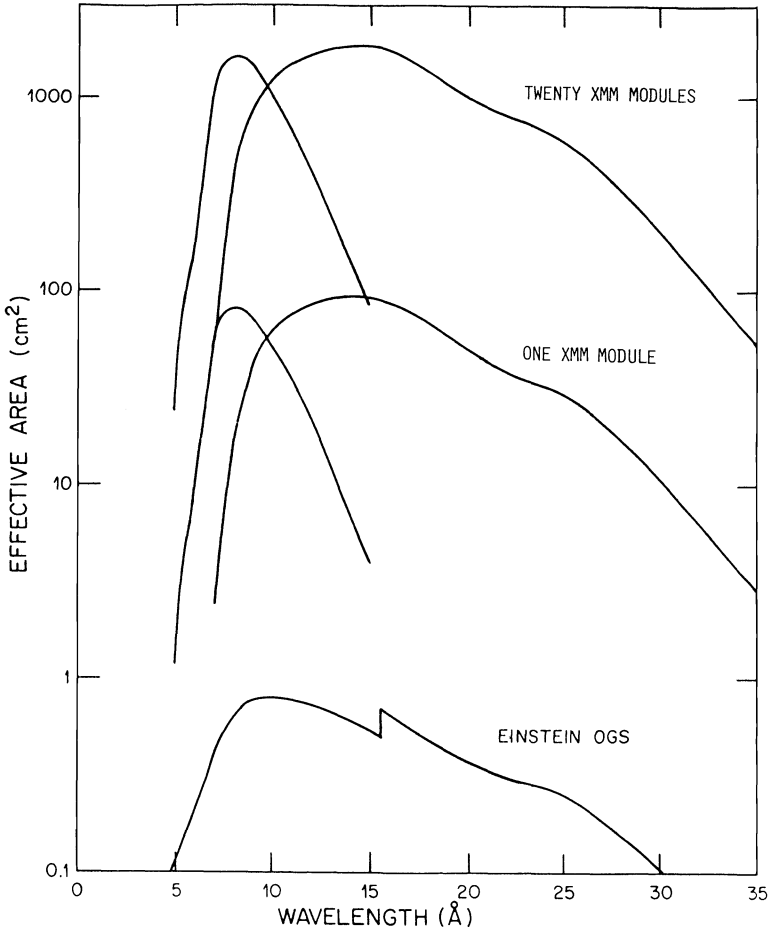

Fig. 6. Effective collecting area in both first and second spectral orders as a function of wavelength, using spectrometer parameters given in Table I. The results for a single XMM telescope-spectrometer instrument (one module) and those for a full twenty module XMM are compared to that obtained with the objective grating spectrometer (OGS) on Einstein.

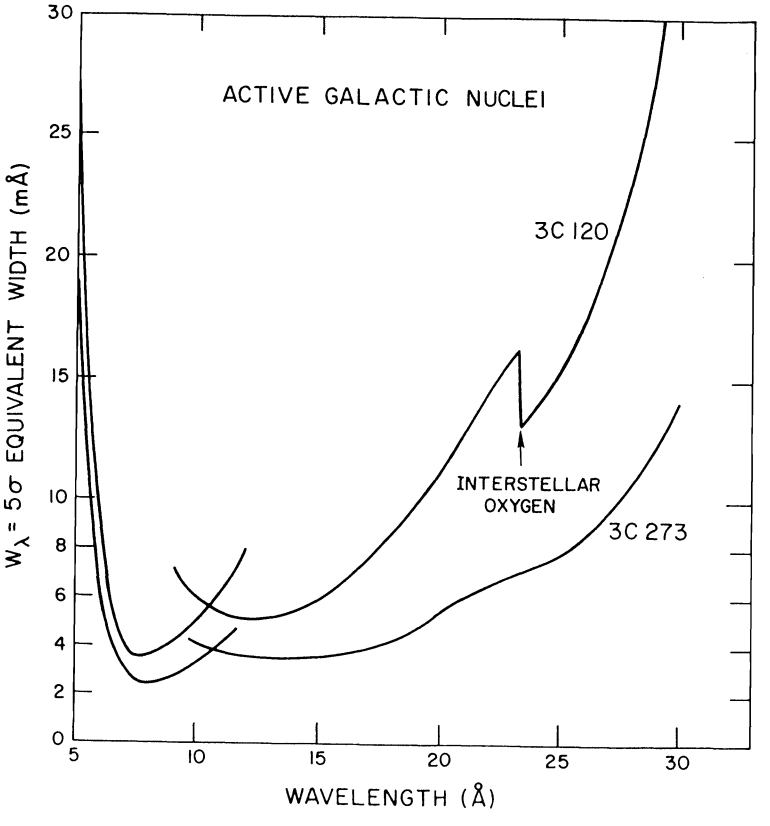

Fig. 7. Sensitivity of the XMM spectrometer array to active galactic nuclei (AGNs). The equivalent widths detectable at a 5σ level are calculated for an AGN with a low intervening column density (3C 273) and for one with a comparatively high column (3C 120). In both cases, a sensitivity of approximately 5 mÅ is obtained from 6-25Å, a band which contains numerous K-shell and L-shell features of abundant elements previously detected in similar sources (x-ray binaries) at 40 times this sensitivity.